An interpretable rule-based system for classification of staining patterns

Sebastijan Dumančić, Antoine Adam and Hendrik Blockeel
Department of Computer Science
Katholieke Universiteit Leuven
3001 Heverlee, Belgium
sebastijan.dumancic@student.kuleuven.be

Abstract— **In this paper we present a new perspective on computer aided assistance in medical domains. As a study case, a diagnosis of autoimmune diseases is taken, where the system should recognize different staining patterns related to specific autoimmune diseases. The emphasis is put on the interpretation of a model, instead of accuracy. The proposed solution is composed of the three consecutive steps - cell segmentation, fluorescence intensity level classification and rule induction. The interpretability of the model is achieved by learning a symbolic representation, with regard to visual appearance, by a Deep belief network. The performance of four commonly used algorithms, `FOIL`, `ALEPH`, `RIPPER` and `Decision trees`, are compared. The performance of the proposed solution is comparable with the state-of-the-art solutions reported so far, but also provides the explanation of decision, which makes it very suitable in computer aided assistance context.**

I. INTRODUCTION

In the last couple of decades, computers have found a number of applications in biology and medicine. We may even say they have become an essential tool in revealing the questions of life. A significant role in those problems was played by machine learning, a branch of artificial intelligence concerned with the construction of models capable of learning from data . Probably the most inspiring example comes from the field of bioinformatics where scientists have used the methods from statistics and artificial intelligence to sequence the human genome for the first time.

Of special interest to this work are computer aided diagnostic systems which offer an assistance to the doctors. Many of diagnostic test are based on a visual interpretation of microscopic images. In the focus of this work is the Antinuclear antibodies test (ANA), which plays the main role in the serological[1] diagnosis of autoimmune disease. ANAs are directed against a variety of antigens and can be detected in patient serum through laboratory tests. ANA test is based on an Indirect immunofluorescence imaging (IIF). Indirect immunofluorescence is a diagnostic methodology based on image analysis that reveals the presence of autoimmune diseases by searching for antibodies in the patient serum. The search is performed by colouring the antibodies.

As it is generally more sensitive than other methods, there has been a growing demand for diagnostic tests for systemic autoimmune diseases. Unfortunately, IIF still remains a subjective method that depends too heavily on the experience and expertise of the physician. The main reasons causing the problems are: the lack of quantitative information supplied to physicians, varieties of reading systems and optics, the photo-bleaching effect caused by a light source irradiating the cells over a short period of time and the low reproducibility of the diagnostic protocol.

The procedure of ANA starts with fluorescence intensity classification, a segmentation step is not a part of ANA procedure. The Center for Disease Control and Prevention in Atlanta,USA have published guidelines [4] for scoring the intensity. The score ranges from 0 to 4+ as follows:

- 4+ : brilliant green (maximal fluorescence)
- 3+ : less brilliant green fluorescence
- 2+ : defined pattern but diminished fluorescence
- 1+ : very subdued fluorescence
- 0 : negative.

Although the guidelines provide very detailed instructions, in [1] Rigon et al. analyzed the variability between a set of physician's fluorescence intensity classifications. Their work has shown a big variance of classifications made by physicians on the same dataset, so they suggested to classify the fluorescence intensity into three classes, namely negative, intermediate and positive. This work follows the protocol.

The final step consists of staining pattern recognition. As shown in figure 1, there are several patterns that may be observed. IIF uses the human epithelial (HEp-2) substrate, which bonds with serum antibodies forming a molecular complex. This complex then reacts with human immunoglobulin [2] and becomes visible under a fluorescence microscope which reveals the antigen-antibody reaction. [2] and [3] provide a description of all staining patterns which is a valuable input taking into consideration a human interpretable perspective of this step. A summary is presented here:

- **Centromere**: characterized by several discrete speckles ($\sim 40-60$) distributed throughout the interphase[3] nuclei and characteristically found in the condensed nuclear

[1]Further explanation

[2]Immunoglobulin is a specific type of antibody created by plasma cells

[3]The interphase is the nonmitotic phase of the cell cycle in which the cell spends the majority of its time and performs the majority of its purposes

chromatin during mitosis as a bar of closely associated speckles.
- **Nucleolar**: characterized by clustered large granules in the nucleoli of interphase cells which tend towards homogeneity, with less than six granules per cell.
- **Homogeneous**: characterized by a diffuse staining of the interphase nuclei and staining of the chromatin of mitotic cells.
- **Fine Speckled**: characterized by a fine granular nuclear staining of the interphase cell nuclei.
- **Coarse Speckled**: characterized by a coarse granular nuclear staining of the interphase cell nuclei.
- **Cytoplasmatic**: characterized by a highly irregular shape and large granule in the nucleoli

The problem contains three main subtasks - cell segmentation, fluorescence intensity classification and pattern classification. The classification task is further divided into two subtasks - symbolic feature representation and rule mining. The rest of the paper is structured as followed. Section II summarizes the previous work in the area. Section III describes the segmentation procedure, while section IV describes the symbolic representation learning. Section V shows how rules are minded and the obtained results, while section VI summarizes the proposed approach and offers some future directions.

II. RELATED WORK

A. SEGMENTATION

In [5] and [6], Huang et al. present an adaptive edged-based segmentation method for automatically detecting outlines of fluorescence cells in IIF images. They have divided the images in two groups : sparse region and mass region cells. The mass region cells are those ones which have a *compact* appearance, that look like a smooth object, while the sparse region cells are those ones for which we can detect multiple object in a cell. The approach trains a classifier to classify each image in the groups and applies different segmentation procedure for each group. In the case of the mass region cells, the cells are segmented using Otsu segmentation method, while in the case of the sparse region cell segmentation is performed by an edge detection. Further they incorporate the watershed segmentation step. After a segmentation step performed by the watershed, the approach merges parts located relatively close and eliminates parts not large enough to represent a cell. If the retrieved number of regions doesn't safisfy the defined criteria, the segmentation step is performed again with different parameter settings determinated by Otsu's thresholding. With proposed approach, approximately 10% of the cells remained undetected.

All aforementioned approaches report similar shortcomings : approximately 10% of cells remained undetected and the inability to separate overlapping cells. The focus of the segmentation part of the Thesis will be on overcoming those problems.

B. FLUORESCENCE INTENSITY CLASSIFICATION

The following step, the intensity level classification, hasn't attracted a lot of scientific research, but has demonstrated remarkable results so far.

In [7], authors propose a system based on *Multi-Layer Perceptrons* and a *Radial Basis Network* for the intensity classification step. That system, which makes use of features inspired from medical practice, shows error rates up to 1%, but it uses a reject option and it does not cast a result in about 50% of cases. In [8] the authors further refine their system. They train three experts, one specialized for each class, with a different set of features. They threat the classifiers similar to the *one-vs-all* approach, so the final decision is made by a classifier most certain in it's decision. The authors report a success rate of 92,6% accuracy.

C. CLASSIFICATION

As this problem was emphasized on the *International Conference on Pattern Recognition 2012* as a contest, this step has been well researched and several very successful methods have been proposed. In [2], Foggia et al. provides a detailed overview of the methods submitted for the contest.

The two most successful methods are explained in [9] and [10]. Both methods used local and global texture descriptors as features, such as local binary patterns, discrete cosine transformation and Gabor wavelets. Both methods also employs the SVM classifier with radial basis functions as kernel for the classification task. They have reported the accuracy of 80 %.

More recently, a new overview of the method was presented by Agrawal et al. in [11]. The authors experimented with the most commonly used features in the previous contest - statistical features, histograms of oriented gradients, shape and size descriptors and texture descriptors. They have chosen the most typical representatives of classifiers, namely Naive Bayes, k-NN, SVM and Random forest. The SVM with Law's textural representation significantly outperformed other classifiers and feature representations. Reported accuracy equals 92.85 %.

The state-of-the-art methods is described in [12]. Wiliem et al. reported the accuracy of 95.5 %. In this paper the authors constructed the texture features by extracting patches of cell's body from both inner and outer region of a cell. The classification is made by the Nearest Convex Hull classifier.

III. SEGMENTATION

In the previous section, the encountered problems with the HEp-2 cell segmentation were mentioned. All of the problems occur due to colouring procedure that is time dependent, so cells expose different properties over an image and some of them remain undetected. Second problem that

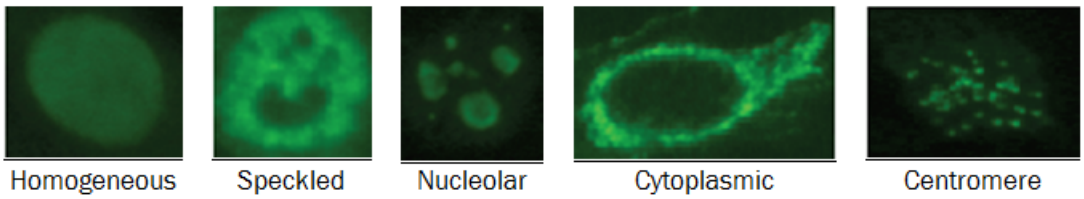

Fig. 1: HEp-2 pattern examples

occur is that a part of the cells overlap. The challenge here is to find a method that can overcome different illumination of objects and separate the overlapping objects. The proposed solution deals with mentioned problems in separate steps.

The method is summarized in Algorithm 1. The proposed solution is based on an observation that, although cells exhibit different properties across image due to different illumination levels, the background is uniform over a whole image and exhibits constant properties. Following the observations, the method first segments the background to find locations of the cells. The background is found by a *Region growing* algorithm. Region growing is a simple method that extends a region based on a similarity in intensity levels - the intensity of each candidate pixel is compared with a mean intensity of a current region. If a difference is less than a given threshold, the pixel is added to the region.

The initial starting region of the Region growing is estimated from an image histogram. As majority of an image is a dark background, every pixel with the intensity value less or equal to the the highest peak in the histogram is automatically declared as background. The threshold is estimated adaptively for each image by approximating the histogram with two Gaussian function. The motivation for such an approximation comes from an assumption that the image histogram should consist of two regions - one modelling the background and a second one modelling cells. Those regions are estimated by approximating the histogram with two Gaussian functions using the EM-algorithm [13]. The threshold is now defined as a distance from the lower mean to the point where two Gaussian are equally probable. An additional restriction that has to be satisfies is that this point should be placed between the means of Gaussians.

For now, we know only the approximate position of objects in an image. To refine the outlines of the cells, the information that most of the cells are circular is used. A *Hough transformation* for circles is used to generate the initial contours for precise outlines. For detailed overview, we refer to [14]. Circles originating in the found background region are considered redundant and are removed because they don't contain any cells. Detected circles are then evolved to better fit the cells with *Morphological snakes* [15]. The idea behind morphological snakes is to represent a curve u in the implicit form and evolve it by solving the system of

Algorithm 1 Segmentation method

```
function SEGMENTATION(image)
    estimate parameters and starting region
    RegionGrowing(image, region, threshold)
    DetectCircles(image)
    remove redundant circles
    for each circle do
        EvolveContour(image, circle)
    end for
end function

function REGIONGROWING(image, region, threshold)
    candidates ← {neighborhood(starting region)}
    currentpoint ← select point from candidates
    while candidates do
        if candidate satisfies criteria then
            add it to region
            add the neighbours to candidates
        end if
        currentpoint ← new point from candidates
    end while
end function

function DETECTCIRCLES(image)
    initialize accumulator H to all zeros
    for each edge in image do
        increment every cell H(x, y, r) which could
        be the center of a circle
    end for
    search for local maxima cells of H
end function
```

partial differential equations (PDE):

$$\frac{\partial u}{\partial t} = \pm|\nabla u| \tag{1}$$

$$\frac{\partial u}{\partial t} = div\left(\frac{\nabla u}{|\nabla u|}\right) \cdot |\nabla u| \tag{2}$$

where $div()$ denotes the divergence operator. Table I summarizes the results compared to the two methods proposed by Huang. It can be observed that this approach leads to significantly improved results with regards to precision and recall. Precision is defined as $\frac{TP}{TP+FP}$ while recall is defined as $\frac{TP}{TP+FN}$, where TP stands for the pixels that are contained both in the ground truth and the segmentation, FP

TABLE I: Pixel level results for each pattern

	Proposed method		MULTISTAGE		AutoLearning	
Pattern	Prec	Rec	Prec	Rec	Prec	Rec
homogeneous	0.961	0.975	0.955	0.58	0.983	0.467
centromere	0.87	0.54	0.628	0.395	0.846	0.356
nucleolar	0.96	0.48	0.667	0.389	0.828	0.44
cytoplasmatic	0.826	0.54	0.166	0.374	0.553	0.269
coarse speckled	0.941	0.977	0.664	0.55	0.928	54.2
fine speckled	0.956	0.94	0.81	0.499	0.941	0.547

TABLE II: Confusion matrices for the shape and fluorescence level classification

(a) Fluorescence intensity

		True	
		pos	**int**
Pred	**pos**	96.50 %	5.75 %
	int	3.50 %	94.25 %

(b) Shape

		True	
		circ	**irr**
Pred	**circ**	99.62 %	6.43 %
	irr	0.38 %	93.57 %

are the pixels that does not belong to the ground truth but are present in the achieved segmentation and FN are the pixels that belong to the ground truth but are not present in the achieved segmentation. Huang's work report approximately 20 % of overlapping cells, while we have observed that 14,53 % remain overlapping with our method.

IV. SYMBOLIC FEATURE GENERATION

Based on the description of certain patterns in section I, symbolic features corresponding with the visual appearance of a pattern are extracted. Those visual features are *shape* - irregular or circular, *speckles* - present or not, *organelle type* - dark, bright or neutral, *number of organelles* - lots, few or none, and *texture* - smooth, sparkly or blob. In addition, the information about the *mitotic cells* presented on an image is assigned to each cells, so as the *fluorescence intensity level*.

The information about the mitotic cells has been manually assigned, while other features, except shape and fluorescence intensity level, are learnt by a *Deep belief network*. Before we explain how the features were assigned with the Deep belief network, we first summarize the classification of a shape and the fluorescence intensity level.

Shape classification. For the shape classification, the segmentation masks are used. The smallest rectangle that can fit the mask is divided in 6 cells - 2 horizontally and 3 vertically. For each cell, a ratio of the background and a cell pixels is calculated and used as a feature. Those 6 features were then used to train the Support vector machine (SVM) [16]. The results are summarized in table II. The achieved accuracy is 98.68 %.

Fluorescence intensity level. The biggest problem with the fluorescence intensity classification is the lack of formal definition of it. It is a subjective parameter that describes the *clarity* of cells in an image.The fluorescence intensity is described with three values - positive, intermediate and negative. The positive value defines images in which cells are perfectly separated from the background, while the negative value defines images in which cells cannot be identified. The intermediate value covers images that are nor positive nor negative.

As the intensity level is correlated with the region growing threshold (section III), a similar approach is taken for this task. The histogram is, in this case, calculated over the smallest rectangle that could fit around a cell. The histogram is approximated with 2 Gaussian functions, and the obtained means and variances are used to train the SVM. The results are presented in the table II. The achieved accuracy is 96.21 % which outperforms the method mentioned in section II.

A. Deep belief network

A *Deep belief network* is an instance of a *Deep learning* methods [17]. Deep learning is a relatively new approach in machine learning which is often referred as Representation learning. It is built upon Artificial neural networks and imitates the human brain in representing data. The motivation for learning representation is quite clear – the form in which data is represented is important. The success of our classifier depends on the quality of data used for training.

The Deep belief network can be seen as a multi-layer generative model where each layer consists of multiple nodes, similar to a neural network. The first layer, often referred as the *visible layer*, represents the raw input data, while every higher-level layer is referred to as the *hidden layer*. It is trained is two steps - first unsupervised then supervised.

For the unsupervised phase, a *Restricted Boltzmann machine* [18] is used. The Restricted Boltzmann machine is a generative energy-based model that shares the parametrization with the neural network. The Restricted Boltzmann machines are trained by maximizing the probability of data:

$$\arg\max_{W} \prod_{v \in V} P(\mathbf{v}) \tag{3}$$

where $\mathbf{v}$ represent a raw data, or visible layer of pixels when trained on images, while probability is represented as an energy

$$P(\mathbf{v}, \mathbf{h}) = \frac{e^{-\mathtt{E}(\mathbf{v},\mathbf{h})}}{\mathtt{Z}} \tag{4}$$

$$\mathtt{E}(\mathbf{v}, \mathbf{h}) = -\mathbf{b}^T\mathbf{v} - \mathbf{c}^T\mathbf{h} - \mathbf{h}^T\mathbf{W}\mathbf{v} \tag{5}$$

where $\mathbf{v}$ represents raw data, $\mathbf{h}$ response of hidden units, $\mathbf{b}_i$ and $\mathbf{c}_i$ are the offsets associated with a single element from $\mathbf{x}$ or $\mathbf{h}$ and $W_{ij}$are weights associated with each pair of units from different layers. $\mathtt{Z}$ is a normalization factor. After unsupervised training, the deep belief network is *fine tuned* by backpropagation [19].

For each of the above mentioned symbolic features - texture, number of organelles, organelles type and speckles or not - one deep belief network is trained. The deep belief network and deep belief approaches proved to be suitable for this task. The results are summarized in table III. For each symbolic feature, more than 90 % of cells are correctly classified. For some features, such as texture and number of organelles, the classes are not balanced, which seems to pose a problem for the deep belief network. Most of these unbalanced classes are highly distinguishing for certain patterns, so it is of interest to recognize them as accurately as possible.

An interesting result is that convolutional layers seem to not improve the accuracy. As convolutional components are developed with image classification in mind, this result is surprising. Only a brief comparison was performed at the beginning to select the most promising model to analyze it with more detail, so there might exist some models with convolutional components that achieve better results.

V. RULE MINING

The output of the previous step is used to mine rules that describe each pattern. For that purpose, four commonly used algorithms - `FOIL`, `ALEPH`, `RIPPER` and `Decision trees` - were compared. The `IF-THEN` rules are the representation of choice because they are easy to understand and very expressive.

`FOIL`, `ALEPH` and `RIPPER` are the *Inductive logic programming*. Inductive logic programming is an intersection between Machine learning and Logic programming where logic representation is used to induce knowledge. Inductive logic programming is concerned with finding a hypothesis $\mathcal{H}$ from a set of positive and negative examples $\mathcal{P}$ and $\mathcal{N}$. It is required that the hypothesis $\mathcal{H}$ covers all positive examples in $\mathcal{P}$ and none of the negative examples in $\mathcal{N}$. They all follow a concept of *sequential covering* - they produce one clause per time that cover as many positive examples as possible and as less negative examples as possible. Although they follow the similar principle, there are some differences how they generate new rules, or detailed overview we refer to [20].

Decision trees are one popular instance of machine learning algorithms due to their *simplicity* and *interpretability*. The decision tree approximates discrete functions and it is very robust to noisy data which makes it suitable for this application. It uses the *tree* structure to represent and compress the data where each *node* represents a test on attribute and each *branch* stands for values of the tested attribute. The decision tree performs a *greedy search* in a search space and chooses an attribute to split data on. The chosen attribute then becomes the node in the tree, and values it can take become branches. As a measure of *quality* of an attribute, *information gain* is used :

$$\texttt{IG}(\mathcal{D}, A) = \texttt{Entropy}(\mathcal{D}) - \sum_{v \in values(A)} \frac{|\mathcal{D}_v|}{|\mathcal{D}|} \texttt{Entropy}(\mathcal{D}_v) \tag{6}$$

where $\mathcal{D}_v = \{x \in \mathcal{D} | A(x) = v\}$ represents a subset of the original data set $\mathcal{D}$ with attribute A equal to v. The entropy is defined as :

$$\texttt{Entropy}(\mathcal{D}) = \sum_{k=1}^{K} p(\mathcal{C}_k) \texttt{log}_2 p(\mathcal{C}_k) \tag{7}$$

where $p(\mathcal{C}_k)$ stands for a fraction of examples in data set $\mathcal{D}$ that belong to class $\mathcal{C}_k$. For details about the decision trees, we refer to [19].

Classifiers are evaluated with the 10-fold cross validation. Tables IV summarizes the precision and recall of each classifier. Results are represented class-wise together with the number of rules found. When analysing the performance of the classifier, both accuracy and the number of induced rules should be considered. The results suggest that `Decision tree` and `RIPPER` perform the best. The overall accuracy of the decision tree and RIPPER are 95.26 % and 94.50 % respectively. The `Decision tree` achieves the highest accuracy, but produces significantly more rules - 25 compared to 10 induced by `RIPPER`. Such a difference suggests overfitting. It can be observed that `RIPPER` not only produces less rules, but those rules are also much simpler than ones induced by the `Decision tree`. Rules induced by `RIPPER` usually have one or two clauses in the body, while rules induced by the `Decision tree` usually have three or four clauses in the body. Also, it can be seen that 9 out of 25 rules induced cover less than 10 examples in the dataset. The state-of-the-art performance reported so far is 95.19 % [12]. The obtained results are quite comparable to their work, but also provide explainable results.

Taking both performance and simplicity into account, the rules induced by `RIPPER` seem to perform the best. Their simplicity makes them more applicable to real life scenarios. They also correspond more to the intuition about the patterns. The induced rules mostly extract the most distinguishing property of a certain pattern. For example, *centromere* class is identified by a large number of objects in the cell body, *cytoplasmatic* by the irregular shape and *coarse speckled* by rough texture. All of these properties are characteristic for specific patterns and don't appear for other types. The drawback of this approach is that rules should be always applied *sequentially*.

Table V summarizes the results obtained when features generated by the deep belief network is used. The performance of `Decision tree` in this case equals 91.34 %, while `RIPPER` classifies 90.51 % of the cells correctly. The effect of a misclassified symbolic features is largely reduced with the information about the mitotic cells.

TABLE III: Symbolic feature mapping

	bright	neutral	dark
bright	93.6 %	0.8 %	5.3 %
neutral	4.3 %	97.2 %	6.7 %
dark	2.1 %	2 %	88 %

a) Organelle Type

	rough	smooth	blob
rough	83.7 %	2.3 %	11 %
smooth	16.3 %	97.7 %	28 %
blob	0	0	61 %

b) Texture

	lots	few	none
lots	82 %	2.3 %	2.6 %
few	8.8 %	89 %	3.7 %
none	9.2 %	8.7 %	93.7 %

c) number of objects

	spec	hom
spec	92 %	10 %
hom	8 %	90 %

d) speckles

TABLE IV: Performance of the algorithms

	Decision tree		RIPPER		FOIL		Aleph	
pattern	Prec	Rec	Prec	Rec	Prec	Rec	Prec	Rec
homogeneous	93.48 %	100 %	93.48 %	100 %	92.15 %	100 %	100 %	69.69 %
nucleolar	97.10 %	97.10 %	94.65 %	95.44 %	97.10 %	88.78 %	97.75 %	72.19 %
centromere	100 %	93.56 %	98.24 %	93.54 %	100 %	92.37 %	100 %	93.22 %
cytoplasmatic	96.46 %	100 %	96.33 %	96.33 %	96.46 %	90.9 %	100 %	100 %
fine speckled	87.00 %	93.27 %	83.33 %	86.54 %	87.00 %	58.57 %	99.09 %	52.4 %
coarse speckled	88.10 %	96.86 %	92.78 %	85.71 %	96.86 %	84.27 %	40 %	1 %
#rules	25		10		17		18	

TABLE V: Performance with features from DBN

		homogeneous	nucleolar	centromere	cytoplasmatic	fine speckled	coarse speckled
RIPPER	Prec	92.94 %	86.40 %	94.67 %	98.02 %	81.40 %	90.91 %
	Rec	99.70 %	92.95 %	89.64 %	90.83 %	84.13 %	80.95 %
DT	Prec	92.94 %	90.94 %	99.70 %	98.98 %	79.05 %	84.47 %
	Rec	99.70 %	95.85 %	93.00 %	88.90 %	79.81 %	82.86 %

VI. CONCLUSION

This paper proposes a solution for computer aided assistance in commonly used diagnostics in autoimmune diseases. The solution closely follows the procedure medical experts suggest. It covers the segmentation task, the fluorescence intensity level classification and staining pattern classification. The strongest contribution of this work is the interpretable approach to prediction models that help medical experts.

Future work include improving the segmentation with model based approaches, mitotic detection, artefact remove and further experiments with the deep learning methods.

REFERENCES

[1] A. Rigon, Indirect immunofluorescence in autoimmune diseases: Assessment of digital images for diagnostic purpose, in Cytometry Part B-clinical Cytometry, vol. 72B, 2007, pp.472–477

[2] P. Foggia et al., Benchmarking HEp-2 Cells Classification Methods, in IEEE Trans. Med. Imaging, vol. 32, pp. 1878-1889, 2013

[3] P. Perner, Mining knowledge for HEp-2 cell image classification, Artificial Intelligence in Medicine, vol. 26, 2002, pp. 161–173

[4] R.M. Nakamura, Quality Assurance for the Indirect Immunofluorescence Test for Autoantibodies to Nuclear Antigen (IF-ANA): Approved Guideline (1996), NCCLS document, NCCLS, 1996

[5] Y.L. Huang et al., Adaptive Automatic Segmentation of HEp-2 Cells in Indirect Immunofluorescence Images, Proceedings of the 2008 IEEE International Conference on Sensor Networks, Ubiquitous, and Trustworthy Computing (Sutc 2008), IEEE Computer Society, pp. 418–422, 2008

[6] Y.L. Huang et al., Outline Detection for the HEp-2 Cell in Indirect Immunofluorescence Images Using Watershed Segmentation, Proceedings of the 2008 IEEE International Conference on Sensor Networks, Ubiquitous, and Trustworthy Computing (Sutc 2008), IEEE Computer Society, pp. 423–427, 2008

[7] P. Soda and G. Iannello, A Multi-Expert System to Classify Fluorescent Intensity in Antinuclear Autoantibodies Testing, 19th IEEE International Symposium on Computer-Based Medical Systems, IEEE Computer Society, pp. 219–224, 2006

[8] P. Soda, G. Iannello and M. Vento, A Multiple Expert System for Classifying Fluorescent Intensity in Antinuclear Autoantibodies Analysis, Pattern Anal. Appl., vol 12, Springer-Verlag, pp. 215–226, 2009

[9] Li Kuan et al, Multiclass boosting SVM using different texture features in HEp-2 cell staining pattern classification, 21st International Conference on Pattern Recognition, pp. 170–173, 2012

[10] Ryusuke Nosaka, Yasuhiro Ohkawa and Kazuhiro Fukui, Feature Extraction Based on Co-occurrence of Adjacent Local Binary Patterns, Proceedings of the 5th Pacific Rim Conference on Advances in Image and Video Technolog, vol. 2, Springer-Verlag, pp. 82–91, 2012

[11] Praful Agrawal,Mayank Vatsa and Richa Singh, HEp-2 Cell Image Classification: A Comparative Analysis, in Lecture Notes in Computer Science, Machine Learning in Medical Imaging, vol. 8184, Springer International Publishing, pp. 195-202, 2013

[12] A. Williem et al, Classification of Human Epithelial Type 2 Cell Indirect Immunofluoresence Images via Codebook Based Descriptors, Proceedings of the 2013 IEEE Workshop on Applications of Computer Vision (WACV), IEEE Computer Society, pp. 95–102, 2013

[13] A. P. Dempster, N. M. Laird and D. B. Rubin, Maximum likelihood from incomplete data via the EM algorithm, Journal of the Royal Statistical Society, series B, vol. 39, pp. 1–38, 1977

[14] P. V. C. Hough, Machine Analysis of Bubble Chamber Pictures, International Conference on High Energy Accelerators and Instrumentation, vol. C590914, pp. 554-558, 1959

[15] P. Marquez-Neila, L. Baumela and L. Alvarez, A Morphological Approach to Curvature-Based Evolution of Curves and Surfaces, IEEE Transactions on Pattern Analysis and Machine Intelligence, vol. 36, IEEE Computer Society, pp. 2–17, 2014

[16] V. Vapnik and C. Cortes, Support-Vector Networks, Machine learning, vol. 20, Kluwer Academic Publishers, pp. 273–297, 1995

[17] Y. Bengio, Learning Deep Architectures for AI, in Found. Trends Mach. Learn., vol. 2, Now Publishers Inc., pp. 1–127, 2009

[18] H. Larochelle and Y. Bengio, Classification using discriminative restricted boltzmann machines, In ICML '08: Proceedings of the 25th international conference on Machine learning, ACM, 2008

[19] K. Murphy, Machine Learning: A Probabilistic Perspective (Adaptive Computation and Machine Learning series), MIT Press, 2012

[20] N. Lavrač and S. Džeroski, Inductive Logic Programming: Techniques and Applications, Routledge, 1993

[21] R. B. Palm, Prediction as a candidate for learning deep hierarchical models of data, Master's Thesis, 2012